Influence of electrical operating conditions and active layer thickness on electroluminescence degradation in polyfluorene–phenylene based light emitting diodes

B. Romero [a,*], B. Arredondo [a], A.L. Alvarez [a], R. Mallavia [b], A. Salinas [b], X. Quintana [c], J.M. Otón [c]

[a] *Dpto. Tecnología Electrónica, Universidad Rey Juan Carlos, C/Tulipán s/n, 28933 Móstoles, Madrid, Spain*
[b] *Instituto de Biología Molecular y Cellular, Universidad Miguel Hernández, Av. del Ferrocarril, s/n Elche 03202 Alicante, Spain*
[c] *Dpto. Tecnología Fotónica, Universidad Politécnica de Madrid, Ciudad Universitaria s/n, 28040 Madrid, Spain*

Keywords:
Polymer light emitting diodes
Degradation
Polyfluorene

A B S T R A C T

We have studied the influence of the electrical working conditions (voltage or current biased), and the active layer thickness on electroluminescence (EL) properties of polymeric light emitting diodes based on poly-[9,9-bis(6′-cyanohexyl)-2,7-fluorene-alt-co-1,4-phenylene], [PFP:$(CN)_2$]. Diodes with different active layer thicknesses (55–140 nm) have been fabricated and characterized. Temporal evolution of the spectra at constant bias and current, as well as the spectral evolution with the current, has been performed. Excitation photoluminescence has been used to discriminate between intrinsic and defect-related transitions. The relative spectral area arising from defects has been quantified by means of Gaussian deconvolution for different device excitations. Active layer thickness has been observed to play an important role on the emissive spectral shape. In thick samples EL tends to resemble fluorescence from the pristine material. In contrast, thinner samples clearly show two additional bands related to defects: the first one is structured in the range 470–510 nm, which is proposed to be due to electron accumulation in the active layer, and a second band at 535 nm, arising from on-chain keto defects due to the presence of oxygen. The role of the electron blocking character of the PEDOT:PSS on the spectral shape, as well as the influence of the active layer thickness on the oxygen concentration, are discussed.

1. Introduction

Since the discovery of polyfluorenes (PFs), they have drawn great attention due to their interesting properties as blue emitters for solution-processable polymer light emitting diodes (PLEDs): high efficiencies, reasonable mobilities and good thermal and chemical stability [1]. Besides, the solubility and processability of these polymers can be easily improved, by substituting the C-9 carbon, without significantly increasing the steric interactions in the polymer backbone, which eventually confers them better performance than other approximations for blue emission using polyparaphenylene (PPP).

Despite PF and copolymers being promising candidates as blue emitting materials, most of the synthesised derivatives have so far a problem related to colour instability, consisting of the development of undesired low energy emission bands during device operation. This has been attributed to a variety of degradation processes, and eventually means a loss of colour saturation. As a result, PFs degradation is currently the main drawback when using these materials as active layers, and consequently, this issue is being the subject of numerous studies [2,3].

Typical blue emission of PF based diodes is dominated by highly efficient intrinsic bands corresponding to the excitonic transition, and a noticeable vibronic splitting up to several orders. Particular interest received an extrinsic green emission band at 530 nm. This band appears after thermal annealing of the polymer film or during device operation, both in air. The initial hypothesis attributed this phenomenon to intermolecular excimer formation between polyfluorene chains [4,5]. Recent experimental evidences have established that the origin of the green emission is related to the presence of fluorenone defects (C=O bonds at the C-9 carbon) in the polymer chain upon thermal or photo-oxidation in the presence of oxygen [6,7]. The relevance of this defect is due to its efficiency as emissive centre, favouring the energy transfer from the fundamental excitonic level. Zhao et al. associated the green band to the formation of an insoluble, cross-linked species that is formed upon thermal degradation and may be enhanced by annealing at high temperatures [8]. Other authors have suggested that fluorenone defects are originated during device processing. In particular, the deposition of low work function metals such as Ca or Ba n-dopes the polymer, and the doped polymer is oxidized during

* Corresponding author. Tel.: +34 (91) 488 7178; fax: +34 (91) 664 7494.
E-mail address: beatriz.romero@urjc.es (B. Romero).

0038-1101/$ - see front matter © 2008 Elsevier Ltd. All rights reserved.
doi:10.1016/j.sse.2008.11.005

device fabrication generating fluorenone defects and thus the appearance of the green band [9].

In addition, another extrinsic band with structure in the range 470–515 nm, has been observed in many PLEDs. Although several authors have detected this structure [8–14] only a few have proposed hypothesis related to its nature. The origin of this peak is still unclear and is subjected to controversy. Gamerith et al. identified for first time this band as being independent on the fluorenone defect. They suggested that it may feature more than one peak, and proposed that it is due to chemical interaction in the presence of oxygen between the polymer and an easily oxidized cathode metal (Ca, Al), although the authors could not determined the exact nature of these interfacial defects [10]. Recently, based on in situ photoluminescence (PL) measurements during cyclic voltammetry in an oxygen-free environment, Montilla et al. proposed that this spectral feature is related to the electrochemical degradation of the polymer, which would generate the appearance of a new cross-linked species that was isolated and analyzed [11]. This reaction does not take place during oxidation (hole injection) but specifically in the presence of an excess of electrons above a critical value, regardless the presence of oxygen.

The goal of this work is to thoroughly study the feature at 470–515 nm in polyfluorene–phenylene-based diodes with different active layer thickness. To do so, we have developed PLED matrix, based on this promising material as active layer. Synthesis and fabrication details are explained in Section 2. The polymer used is a new derivative of poly(2,7-fluorene-alt-co-1,4-phenylidene) (PFP), which presents a cyanide group as a final functional group of the hexyl chain at the C9-position of the fluorene ring, (PFP:$(CN)_2$).

Diodes with different active layer thickness, ranging from 55 nm up to 180 nm, have been fabricated, in air or inert atmosphere. Characterization results are provided in Sections 3 and 4. Electroluminescence (EL) was characterized under diverse bias conditions, observing different patterns when changing the active layer thickness. Emission and excitation PL spectra have been recorded inside and outside diodes in order to identify different chemical species. We have also used the analysis of Gaussian deconvolution to obtain quantitative information on defects as evolving with operational conditions. Eventually, in Section 5, two different mechanisms are proposed and discussed in order to explain spectral changes: on one hand, the accumulation of electrons favoured by the slight blocking character of the PEDOT:PSS interface is sensitive to the active layer thickness, and may in turn modify the recombination zone. On the other hand, it is considered that the remained oxygen concentration inside the sample decreases when increasing the active layer thickness.

2. Fabrication procedure

Indium tin oxide (ITO) was used as anode and Poly(3,4-ethylenedioxythiophene)/poly(4-styrenesulfonate) (PEDOT:PSS) was used as hole injection layer, in order to improve the electrical performance. The final device structure is ITO/PEDOT:PSS/PFP:$(CN)_2$/Al.

Device fabrication includes three steps: synthesis of the new material, thin film preparation (thickness calibration), and device processing. Every step is described below.

2.1. Synthesis

Poly-(9,9-bis(6′-cyanohexyl)-2,7-fluorene-alt-co-1,4-phenylene) (Fig. 1) was synthesized via a Suzuki coupling reaction using 1,4-phenyldiboronic acid and 2,7-dibromo-9,9-bis(6′-cyano)fluorene with high yield [15]. The batch of the polymer has an average molecular weight of $M_W = 5.6 \times 10^4$ g/mol, corresponding to around 100 monomer units per polymer chain, and the index polydispersity was 1.95. The introduction of the phenylene group in the conjugated chain results in a 0.2 eV lowering of the LUMO with respect to the typical value in PFs [15], which enables easier electron injection.

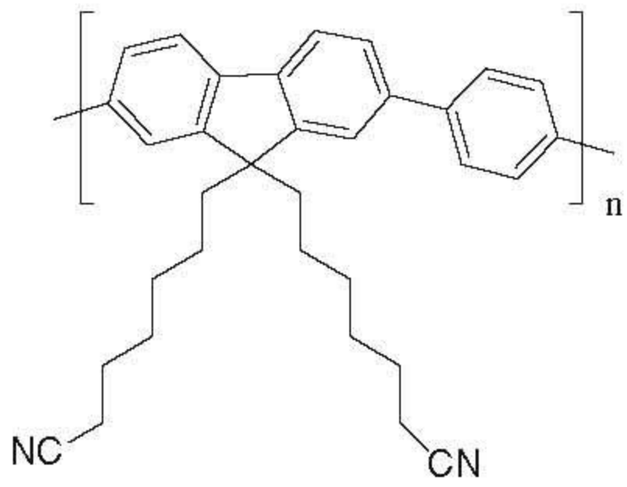

Fig. 1. Chemical structure of PFP:$(CN)_2$.

2.2. Solution and thin film preparation

It is well known that spin-casted film thickness is mainly influenced by the solution concentration. Solutions in tetrahydrofurane (THF) were heated (just below the boiling point) and introduced in an ultrasonic bath during 1 h in order to improve the solubility of the polymer in the solvent. Subsequently, they were filtered through a 0.45 μm filter before being spin-casted at 6000 rpm during 30 s onto a glass substrate. Finally they were annealed at 80 °C during 30 min.

Film thickness was determined using an Alpha-Step 200 contact profilometer.

2.3. LED fabrication

The entire fabrication process is carried out in a clean room (class 10,000). Commercial indium–tin-oxide (ITO, thickness = 100 ± 5 nm) coated glass is used as substrate. Prior to film deposition, the substrates went through a typical organic material cleaning process. The final diode passive matrix contains eight diodes with two different radii, 0.5 and 0.75 mm, consisting of a common cathode, aluminium (Al), and an ITO anode.

The fabrication process consists of several steps. The ITO coated glass is patterned by means of a photolithographic process. In a second photolithographic process, wells in the photoresist are dug on top of ITO pads. The insulating behaviour of the photoresist avoids leakage currents between adjacent diodes. Next, a hole transport layer, poly(3,4-ethylenedioxythiophene)/poly(4-styrenesulfonate) (PEDOT/PSS), is spin-casted at 6000 rpm and dried at 110 °C for 30 min. Such material is insoluble in organic solvents and therefore prevents the photoresist to be dissolved by the solvent of the active polymer. The organic active layer, a solution of PFP:$(CN)_2$ in THF, is spin-casted at 6000 rpm and annealed at 80 °C for 30 min. The Al cathode is thermally evaporated on top of the organic layer surface in an atmosphere of 10^{-6} Torr. Fig. 2a shows the layer structure. Devices are encapsulated using a glass cover attached by a bead of epoxy adhesive. This process is carried out in a glove box under N_2 atmosphere. Finally, contact wires are indium soldered. The final device is the eight diode passive matrix shown in Fig. 2b. Biasing is provided through an ITO path that connects each contact to the outer wire.

3. Electrical and optical characterization

Current–voltage (I–V) characteristics were recorded using an Agilent 4155C semiconductor parameter analyzer and an Agilent

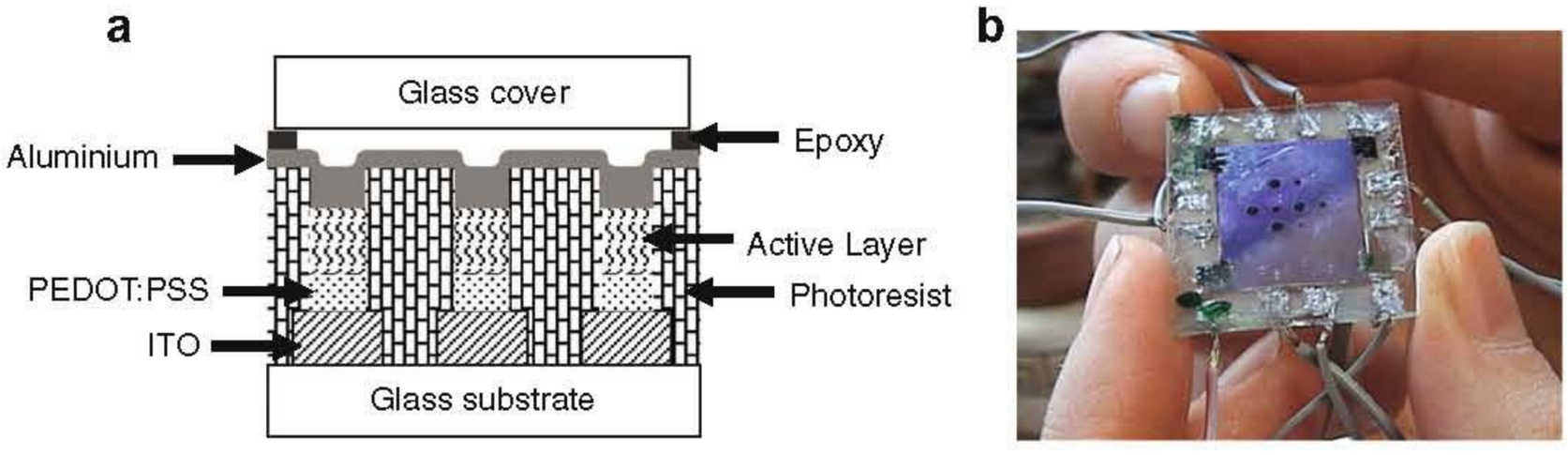

Fig. 2. (a) Layer structure of the fabricated devices. (b) PLED passive matrix.

41501B SMU pulse generator. The samples were pulsed biased. The pulse width was set to 0.5 ms and the duty cycle was 0.5%, in order to minimize device degradation.

EL spectra were recorded using a CS-1000 Minolta Spectroradiometer. Samples were voltage driven with a pulse train with the same pulse width and duty cycle used in the electrical measurements (0.5%).

Steady-state emission and excitation spectra were acquired at room temperature using a PTI QuantaMaster Model QM-62003SE spectrofluorimeter for different devices using a solid support well-adjusted (or aligned) light beams.

4. Results

4.1. Electrical behaviour

Fig. 3 shows the current density–voltage (J–V) for devices with different active layer thicknesses, ranging from 55 nm to 180 nm. As was expected, threshold voltage increases with active layer thickness, but not only due to the limiting effect of the bulk current, but also due to a decrease of the injection rate, associated to a reduction of the internal electric field at the interface [16].

Although the best device, in terms of lowest threshold voltage is the thinnest one, we have checked that the probability of having short circuits increases when the active layer thickness goes below 40 nm, in agreement with [17]. In our case, devices with active layers of 55 nm show even better success probability, in terms of optical lifetime, than those with a thicker active layer.

4.2. Optical behaviour

In Fig. 4, emission and excitation PLs (recorded at 420, 444 and 470 nm) have been performed in a pristine 55 nm layer. The emission PL curve shows one peak at 420 nm corresponding to the excitonic transition, as well as two features at 444 and 470 nm. The first one is typically attributed to the first vibronic peak, and the latter is tentatively assigned to a second order vibronic replica, supported by the coincidence in the energy shift (around 155 meV). The fact that no significant differences have been found in the excitation PL measurements at these wavelengths indicates that the optical response arises from the same intrinsic material and supports the previous assumption. Attending to this, three Gaussian curves will be used in this range when decomposing EL measurements, in order to take into account every intrinsic transition.

Fig. 5 shows two different EL spectra recorded from identical structural devices (around 55 nm active layer thickness). The only difference in the fabrication process took place during the active layer annealing: while sample (a) was cured in N_2 atmosphere, sample (b) was cured in air atmosphere. The shorter wavelength region is dominated by two well resolved peaks at 423 nm and at

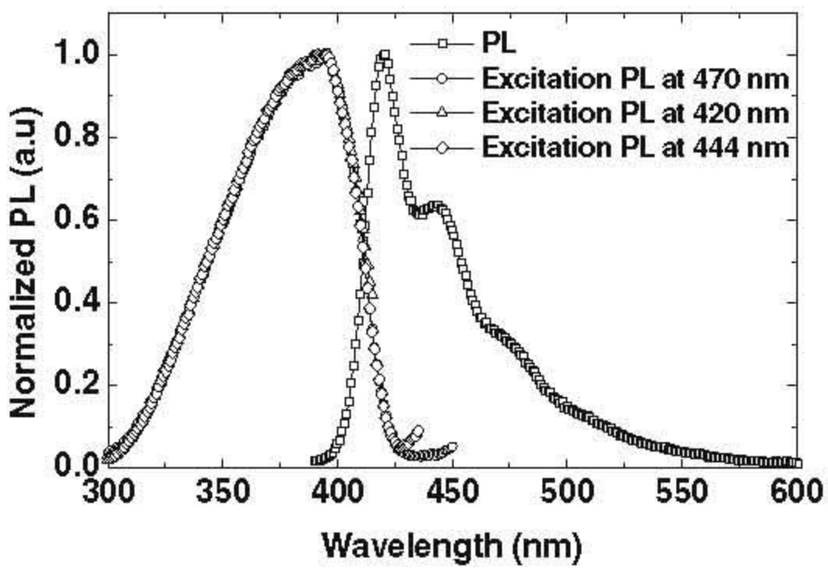

Fig. 4. Normalized emission and excitation PL at 420, 444 and 470 nm for a 55 nm PFP:$(CN)_2$ layer.

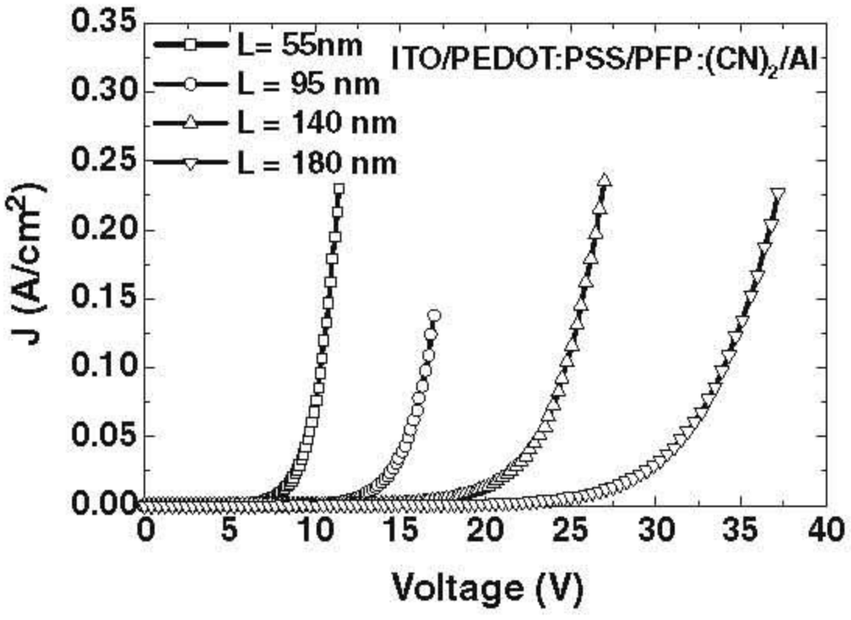

Fig. 3. J–V characteristics of PFP:$(CN)_2$ based diodes with different active layer thicknesses.

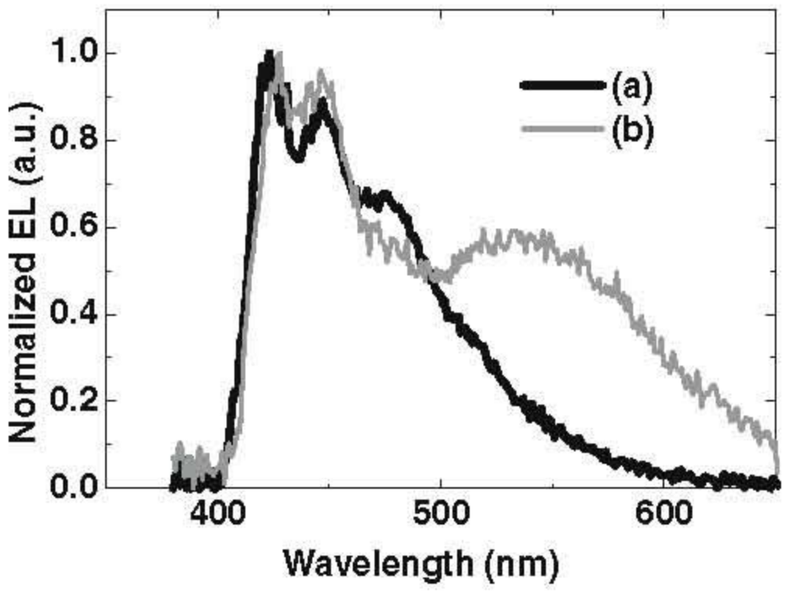

Fig. 5. Normalized EL for diodes cured in (a) N_2 and (b) air.

445 nm, corresponding to the excitonic and first order vibronic transitions, respectively. A well known broad band centred at 535 nm is observed in the air-cured sample (open circles), while this feature is less pronounced in the N_2 dried sample (solid circles). As explained above, this is in agreement with the theory that attributes this band to the incorporation of oxygen as C–O bonds in the polymer backbone, during the fabrication process.

It is worth noticing the appearance of an additional feature at around 470 nm in both spectra, which, despite matching the wavelength of the second order vibronic replica, shows an excessive intensity in the absence of oxygen. In order to thoroughly study these defect-related bands, three different experiments have been designed: in (a) EL spectra were recorded at a constant voltage during several hours of operation, in order to study the temporal evolution of the electrical response and the spectral shape (b) EL spectra were recorded applying a constant current, which will help to discriminate between pure electrical and electro-optical degradation. (c) EL spectra were recorded increasing the bias current.

4.2.1. Spectral evolution at a constant voltage

EL spectra were recorded at a constant voltage during several hours of operation, in order to study the temporal evolution of the electrical response and the spectral shape. Fig. 6a shows the evolution of the EL recorded from a thick (140 nm) active layer diode, along 6 h of operation. The bias voltage was set to 24.4 V, just above the onset for EL (notice that active layer thickness is 140 nm). As can be observed, the spectra are mainly composed by the excitonic band centred at 423 nm, a vibronic shoulder at 445 nm, and a second vibronic replica at around 470 nm. Bands associated to the previously mentioned defects (from 470 nm to 530 nm) are hardly observed in these spectra. Apparently, thicker samples seem to be less affected by extrinsic factors such as electron accumulation, oxygen and moisture. This will be discussed in Section 5.

The total luminance decayed at a half of the initial value after 3 h of operation (Fig. 6b), but no changes in the spectral shape are observed, except for a smooth broad band at 590 nm. By monitoring the device current, it has been checked that the decrease of the luminance is due to a proportional current reduction. This is not accompanied by significant changes in the spectral shape and thus is identified only as pure electrical degradation. This effect may be attributed to a loss of ohmic injection at the polymer/PEDOT:PSS interface (stressing) [18]. Recent investigations have demonstrated that trapped water in the organic layers (PEDOT:PSS is an emulsion in water) is a major source of electrical instability [19].

EL spectra were recorded applying a constant current, adjusting the voltage level in time, which will help to discriminate between pure electrical and electro-optical degradation. Fig. 7a shows the evolution of the EL from a thin (55 nm) active layer diode, along almost 3 h of operation, setting the bias current to 4.3 mA. Mathematical decomposition, assuming Gaussian shapes for the energy transitions, has been performed. It should be pointed out that, although spectra are plotted as function of wavelength, Gaussian deconvolution was performed in the energy domain. Generally, the pristine EL spectra can be reasonably well described by three intrinsic peaks at 420 nm (excitonic), 445 nm (first vibronic) and 470 nm (second vibronic) while degraded spectra need the contribution of two additional extrinsic peaks that account for the structured electro-optical degradation band [20] as well as the fluorenone band. Attempts to include other additional Gaussians in this spectral region were discarded since they did not lead to a

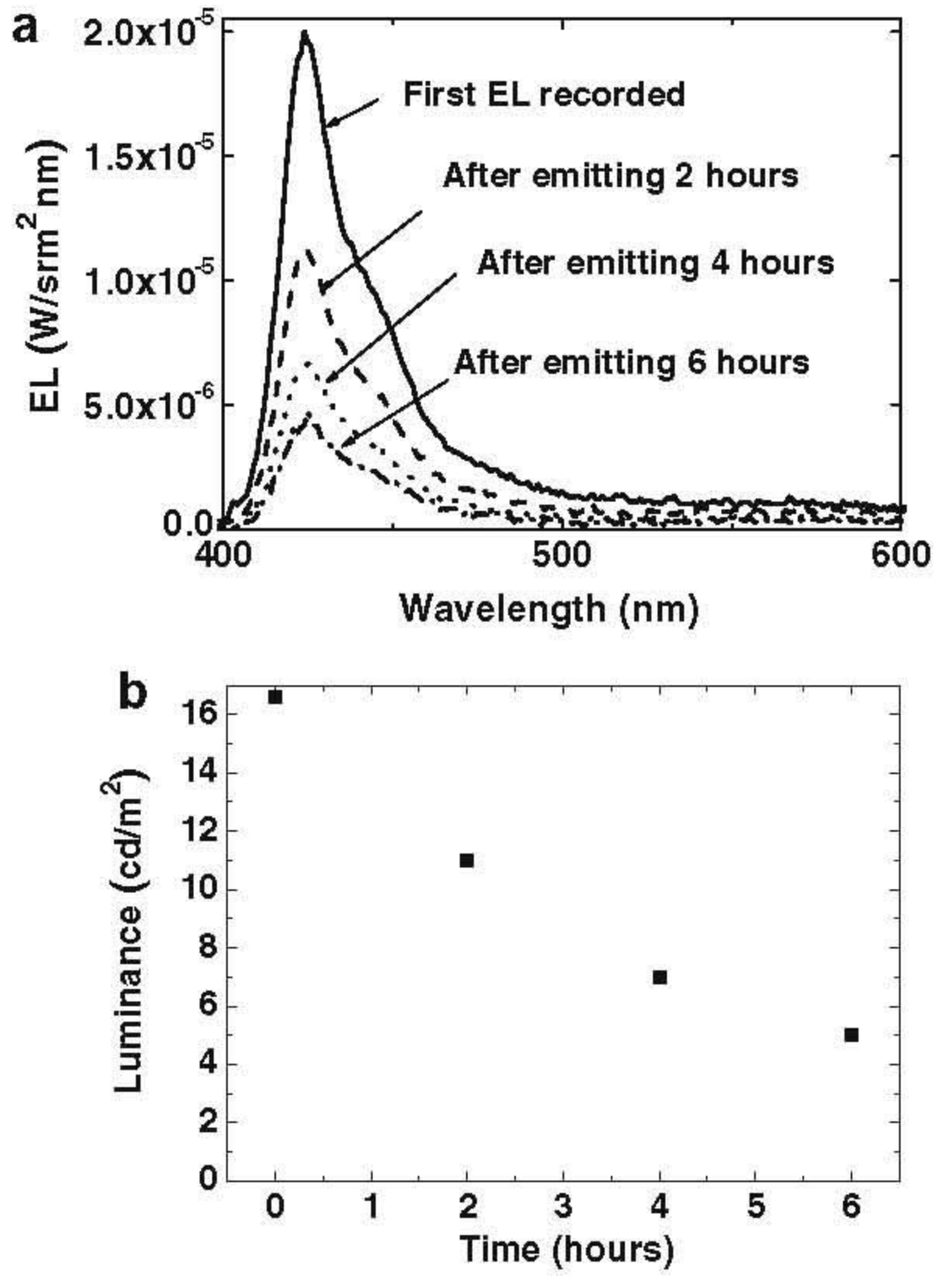

Fig. 6. (a) EL spectra evolution for a 140 nm sample during 6 h and (b) luminance (cd/m^2) vs. time of operation at a constant voltage (24.4 V).

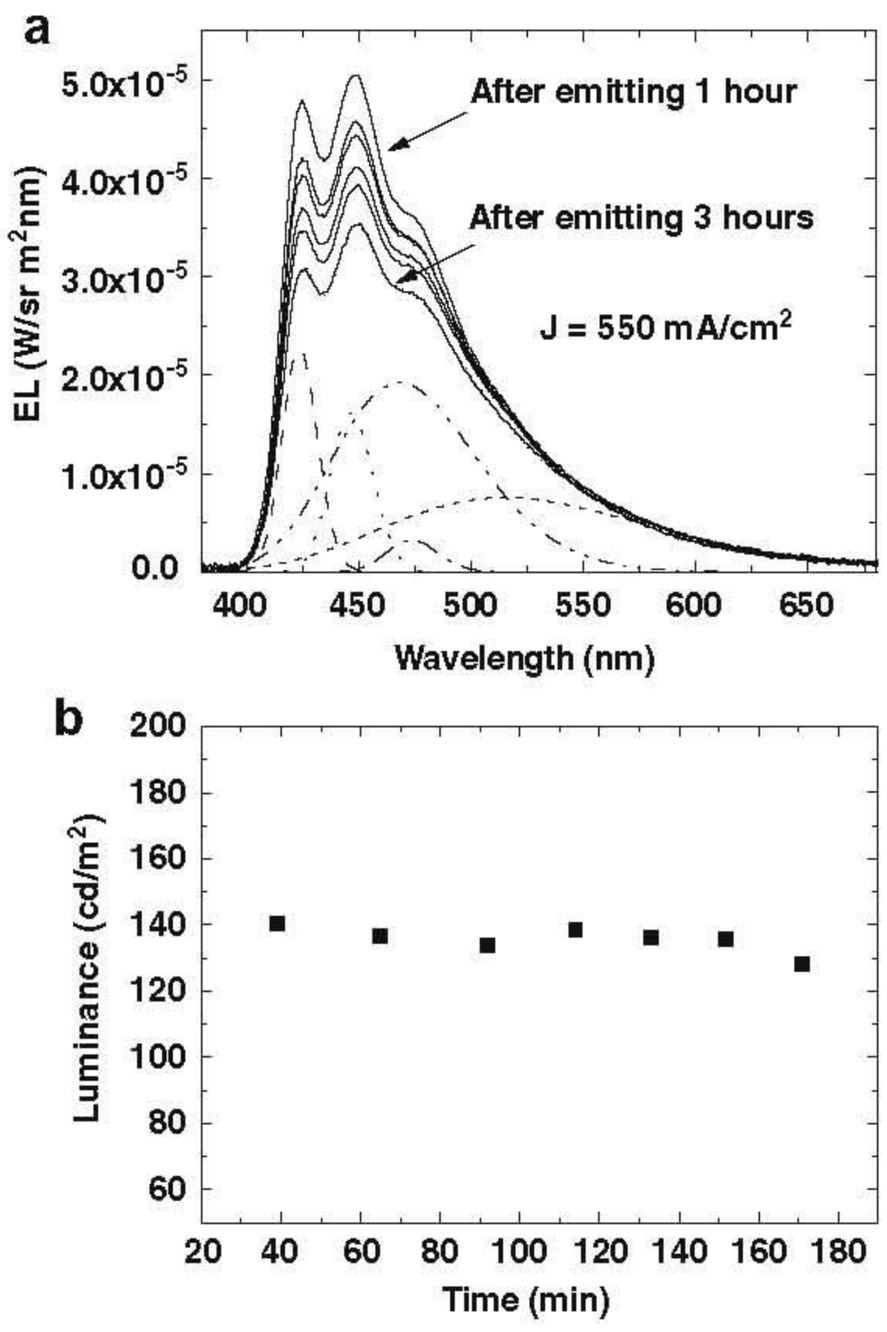

Fig. 7. (a) EL spectra evolution for a 55 nm sample driven at a constant current density (550 mA/cm^2) during 3 h. Spectra are recorded every 20 min. Gaussian deconvolution corresponds to the last spectrum and (b) luminance vs. time of operation for the same sample.

unique solution. Fig. 7a shows this decomposition for the last spectrum (dashed lines) showing that the apparent height increase of the vibronic peak at 445 nm is mainly due to the influence of the extrinsic feature at 470 nm. In fact, the vibronic/excitonic intensity ratio holds rather constant along time.

After several hours of operation, it may be noticed that the shoulder at 470 nm enhances, similarly as observed when an excess of electron concentration remains inside the active layer [11]. In fact, after 3 h of operation, the intensity of this shoulder almost reaches that of the excitonic peak. For this reason, the excitation PL at different wavelengths (420, 470 and 538 nm) have been performed over a degraded diode (55 nm thick). In contrast to the results obtained in a pristine material, a slight difference between the excitation PL recorded at 470 nm (dotted) and that at 420 nm (the intrinsic emission, dashed) is found, supporting the hypothesis of the existence of a new chemical species. This difference becomes stronger for the excitation PL recorded at longer wavelengths such as 538 nm (see Fig. 8).

Also, we observed that the luminance is kept cuasi-constant along time (see Fig. 7b).

4.2.2. Spectra evolution with current injection level

EL spectra were recorded increasing the bias current in order to clarify the study of each transition separately. This experiment, which implies a severe degradation, has been carried out in three different samples: (i) air-cured thin samples (55 nm), (ii) N_2 cured thin samples (55 nm) and (iii) N_2 cured thick samples (140 nm).

Fig. 9 shows the normalized EL spectra, together with its Gaussian deconvolution, for a 55 nm sample cured under air atmosphere at two different injection bias levels. As can be observed, the intensity associated with the 470 nm Gaussian has been promoted by increasing injection level.

For the 55 nm sample cured in N_2, current density was varied from 40 mA/cm^2 up to 1400 mA/cm^2. Fig. 10a–c shows the normalized spectra, together with their Gaussian deconvolutions, for three different current density levels: 40 mA/cm^2, 400 mA/cm^2, and 1400 mA/cm^2. A quick look at the EL reveals that the relative contribution of the defect structured band (from 470 to 510 nm) increases with current. The Gaussian deconvolution confirms this fact, as is shown in Fig. 10d, where the sum of the relative spectral area of the defect bands is plotted vs. current density. Notice that the greatest changes take place at initial currents, and eventually tend to saturation, when most of the material is already degraded.

Fig. 11 shows EL of the 140 nm sample, cured under identical conditions as the 55 nm sample, for different current density levels. The spectra, when compared to previous ones, clearly show that the studied defect bands are much less pronounced in thicker

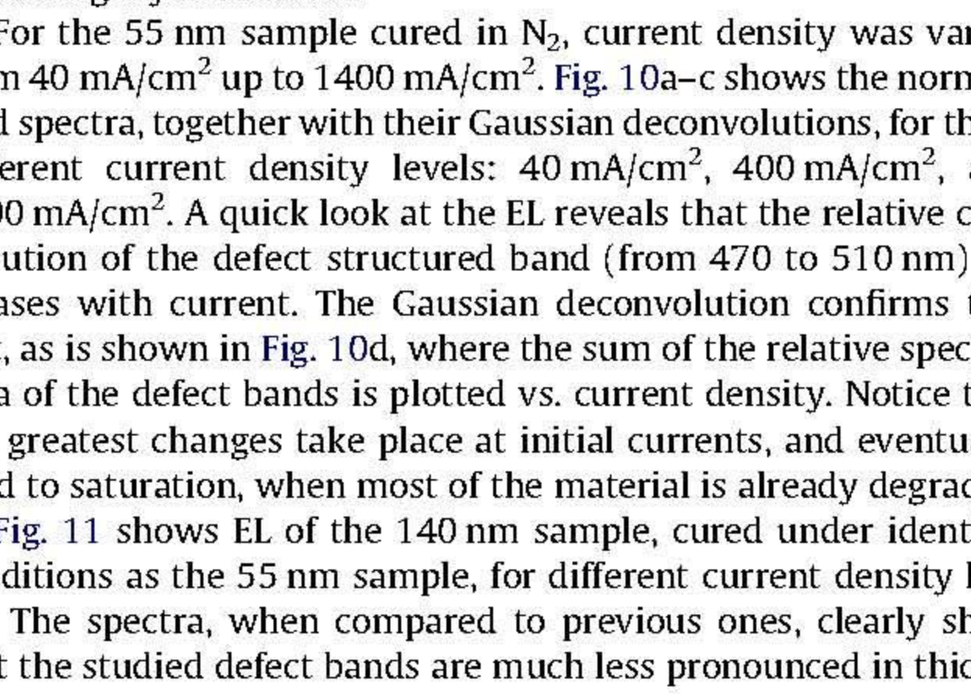

Fig. 8. Normalized emission and excitation PL (at 420, 470 and 538 nm) for a 55 nm PFP:$(CN)_2$ degraded diode.

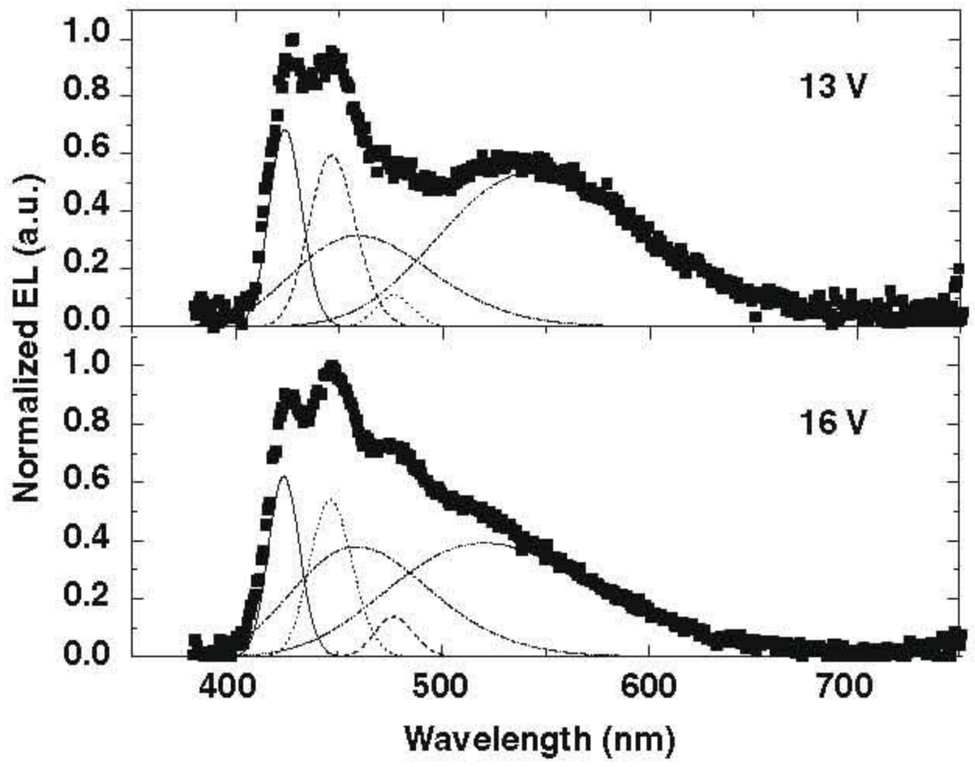

Fig. 9. EL spectra of a 55 nm sample cured under air atmosphere for two bias voltage levels.

samples than in thinner ones, even when the increase of carrier density is one order of magnitude. Instead, a new broad band centred at around 590 nm emerges, which is correlated to material damage upon optical inspection of the device. This will be discussed in next section.

5. Discussion

Previous results pose several questions that will be discussed below. The first one is related to the changes of the EL spectral shape with the active layer thickness. The second one concerns the appearance of the electrooxidation feature between 470 and 510 nm with increasing bias current.

Majority carriers (holes) are injected from the metal contact into the bulk by a jumping process in which the interface electric field helps to overcome the injection barrier between the tandem (ITO/PEDOT:PSS) and the active layer [21]. Holes are then transported mainly by hopping along the bulk, and those that do not recombine or accumulate as space charge, are evacuated through the cathode. This means that, at a certain time, the steady current generates a residual (generally small, for the high energy barriers considered) hole density inside the device that depends on the mobility value. In contrast, the scenario for transport of minority carriers (electrons) is very different. At a sufficient high voltage, they are injected from the cathode (Al) into the active layer. Electrons are transported along the active layer (PFP) and those that do not recombine reach the PEDOT:PSS and presumably accumulate due to its relative good electron blocking properties [22]. The blocking character is not only favoured by the interface barrier (level alignment) but also by a reduction of carrier mobility in the PEDOT: PSS [23]. In this sense, the negative ionic character of the PSS is expected to block the electron path.

In the case of thin samples, electrons have to cover a small distance before reaching the PEDOT:PSS, reducing the probability that an electron recombines in the PFP layer, and then favouring an accumulation due to the PEDOT:PSS interface. This may shift the recombination zone towards that interface, as observed in multilayer structures [24]. Eventually, the electron density increase will enhance the degradation mechanisms, promoting the 470 nm peak in the EL spectra. This is supported by cyclic voltammetry studies that reveal that the 470 nm peak arises from new chemical species that appear as a result of an excess of electrons [11]. On the contrary, increasing the active layer thickness raises the probability that an electron recombines in the PFP layer, lowering the electron

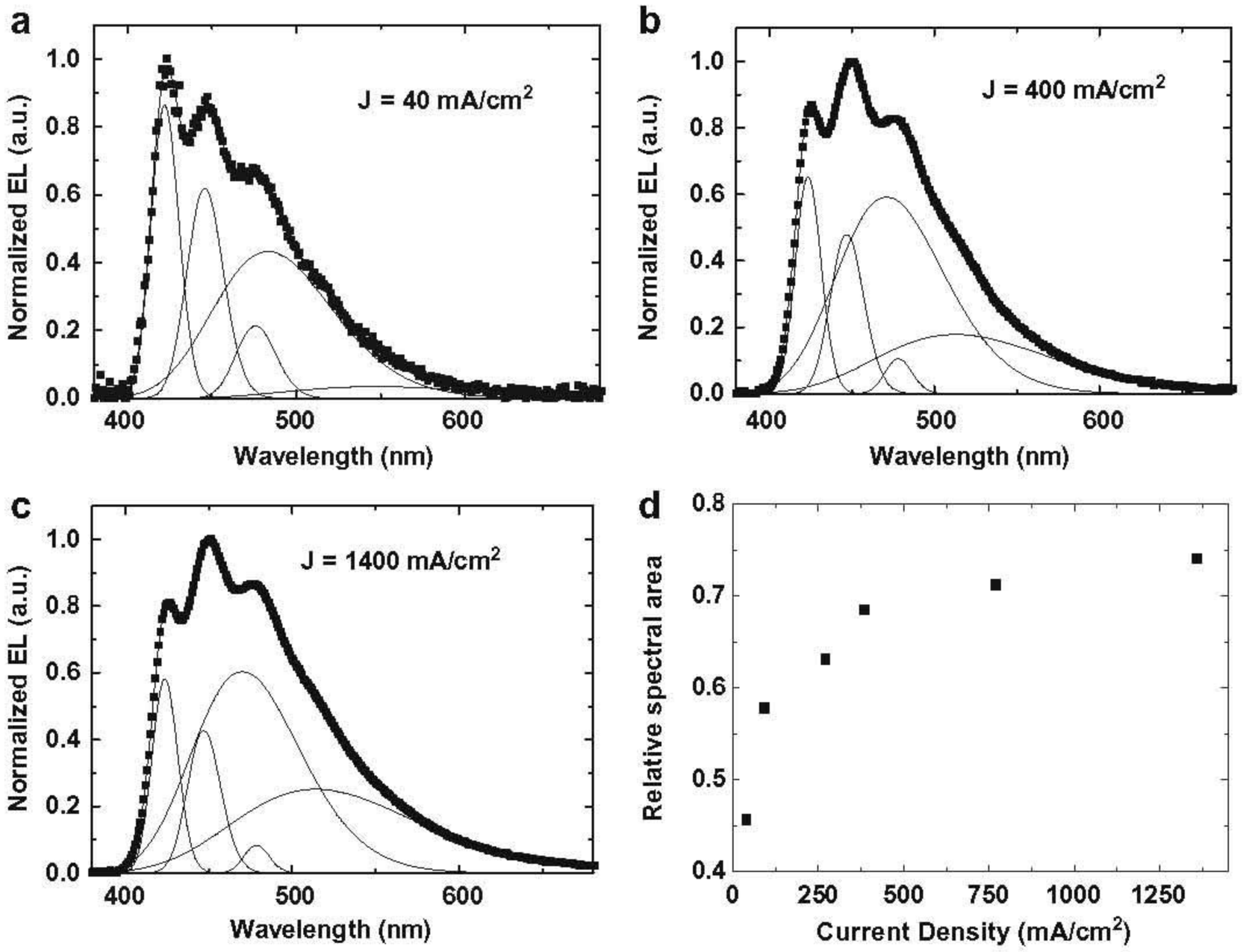

Fig. 10. Normalized EL spectra for a 55 nm sample at different current levels: (a) 40 mA/cm^2, (b) 400 mA/cm^2, and (c) 1400 mA/cm^2. In (d) the sum of the relative defects area is plotted vs. bias current.

accumulation effect due to the PEDOT interface, and thus, diminishing degradation and extrinsic peaks in the EL spectra.

On the other hand, it has been mentioned the reactivity of polyfluorene derivatives in the presence of oxygen. Many studies have proven the formation of the fluorenone upon reaction with the C-9 carbon, resulting in an emissive band centred at 530 nm. In this context, it seems interesting to study the influence of the active layer thickness on this degradation mechanism. To the best of our knowledge, no research has been performed to study the oxygen diffusion length in polyfluorene layers. Few studies on the incorporation of oxygen via creation of free radicals in polymers such as PMMA and PVA reveal diffusion coefficients of the order of 10^{-12} m^2/s [25], which guarantee fast oxygen diffusion in these materials. In fact, the average diffusion distance, $\langle d \rangle$, scales with diffusion coefficient, D, and time, t, as $\langle d \rangle = \sqrt{Dt}$, (according to the Flick's Law), resulting in a diffusion distance of 1 μm in 1 s of exposure. In this context, Gammerith et al. performed an in situ PL study during thermal polyfluorene oxidation, and observed that changes due to creation of defects took place in a few seconds [10]. Regardless the oxygen diffusion length in polyfluorenes, a thickness increase of the active layer decreases the effect of oxygen in the polymer, as may be concluded from two considerations:

(a) In the case the oxygen diffuses along the entire layer, a thicker sample would contain a lower oxygen concentration for the same exposure time.
(b) In the case the oxygen diffuses up to a distance close to the cathode, a thickness increase of the active layer favours that most of the recombination takes place far from that region.

The second remaining question is why the electroxidation feature at 470 nm is less pronounced in thick samples despite increasing bias current.

In the same framework of the previous explanations, it may be proposed that for thick devices, and even in the case of high bias currents, the probability of an electron to recombine inside the active layer is higher than in thinner samples, diminishing the risk of accumulation at any interface, and thus, reducing the appearance of the electrooxidation peak in the EL spectra.

In practice, the determination of the active layer thickness is a critical issue when designing an OLED. Previous observations suggest that thick active layers, above 100 nm, result in better spectral definition (colour saturation). However, increasing thickness requires higher operating voltages as it was previously shown in Fig. 3. Therefore, a trade off between threshold voltage and colour definition should be achieved when designing the optimum active layer thickness, depending on the device application requirements.

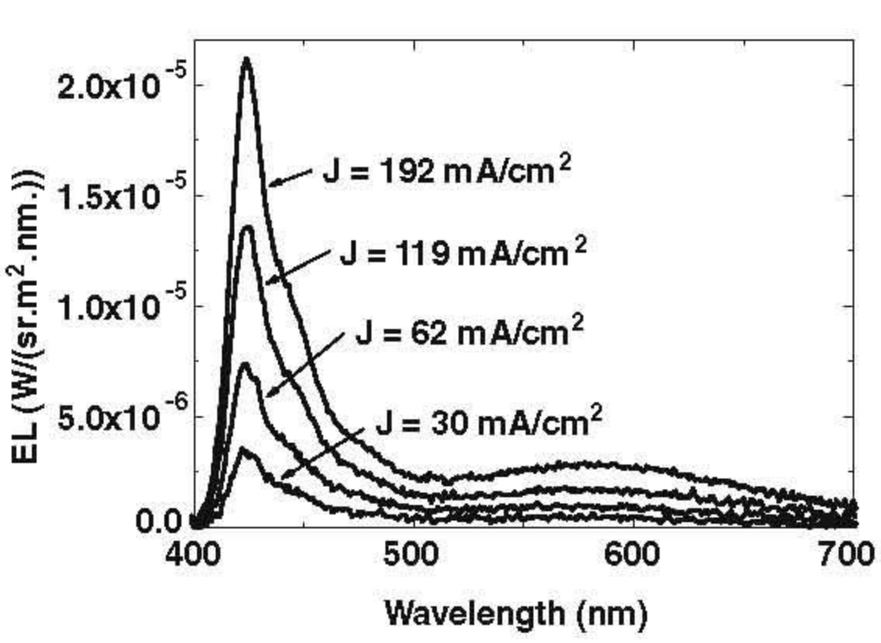

Fig. 11. EL spectra for a 140 nm sample at different bias current density levels.

6. Conclusions

In this work, several electrical treatments have been performed on diodes with different active layer thickness, based a new ciano-

derivative of the polyfluorene–phenylidene, in order to discriminate between different degradation mechanisms. We have recorded EL, emission and excitation PL spectra to identify and quantify main intrinsic and extrinsic emissive bands, with the aid of spectral energy Gaussian deconvolution.

Our experiments show that the structured band in the 470–510 nm region arises from a defect, that may be unintentionally enhanced when device layer structure is not optimized. When this structure favours electron accumulation (as a result of having, for example, an electron blocking layer, such as PEDOT:PSS) this band is clearly enhanced during device operation. This effect may be reduced by increasing the active layer thickness, so that electron accumulation lowers, due to a higher recombination probability along the active layer. The same trend in the fluorenone related defect is observed when increasing active layer thickness: thicker samples contain a lower oxygen concentration resulting in a less pronounced peak at 530 nm.

These results lead to a trade off between optical and electrical performance in PLEDs: When designing device layer structure it should be considered that thinner samples result in low threshold voltages but in higher probability of extrinsic peaks in EL spectra.

Acknowledgements

The authors would like to thank Drs. M. Clement, J. Olivares and F. Calle for thickness measurements. This work was supported in part by Comunidad Autónoma de Madrid under Project S0505/ESP/000417 and in part by the Spanish Ministry of Education and Science under Projects TEC2006-13392-C02-02/MIC and MAT-2005-1004.

References

[1] Bernius MT, Inbasekaran M, O'Brien J, Wu WS. Progress in light emitting polymers. Adv Mater 2000;12:1737–50;
Scherf U, List EJW. Semiconducting polyfluorenes. Towards reliable structure–property relationships. Adv Mater 2002;14:477.
[2] List EJW, Guentner R, de Freitas PS, Scherf U. The effect of keto defect sites on the emission properties of polyfluorene-type materials. Adv Mater 2002;14:374–8.
[3] Montilla F, Pastor I, Mateo CR, Morallón E, Mallavia R. Charge transport in luminescent polymer studied by in situ fluorescence spectroscopy. J Phys Chem B 2006;110:5914–9.
[4] Bliznyuk VN, Carter SA, Scott JC, Klarner G, Miller RD, Miller DC. Electrical and photoinduced degradation of polyfluorene based films and light emitting devices. Macromolecules 1999;32:361.
[5] Sims M, Bradley DDC, Ariu M, Koeberg M, Asimakis A, Grell M, et al. Understanding the origin of the 535 nm emission band in oxidized Poly(9,9-dioctylfluorene): the essential role of inter-chain/inter-segment interactions. Adv Funct Mater 2004;14:765.
[6] Gaal M, List EJW, Scherf U. Excimer or emissive on–chain defects? Macromolecules 2003;36:1750.
[7] Romaner L, Pogantsch A, de Freitas PS, Gaal M, Zojer E, List EJW. The origin of green emission in polyfluorene-based conjugated polymers: on-chain defect fluorescence. Adv Funct Mater 2003;13:597.
[8] Zhao W, Cao t, White JM. On the origin of green emission in polyfluorene polymers: the roles of thermal oxidation degradation and crosslinking. Adv Funct Mater 2004;14:783.
[9] Gong XO, Iyer PK, Moses D, Bazan GC, Heeger AJ, Xiao SS. Stabilized blue emission from polyfluorene-based light-emitting diodes: elimination of fluorenone defects. Adv Funct Mater 2003;13:325.
[10] Gammerith S, Nothofer HG, Scherf U, List EJW. Identification of emissive interface-related defects in polyfluorene based light emitting devices. Jpn J Appl Phys Part 2 2004;42:891.
[11] Montilla F, Mallavia R. On the origin of green emission bands in fluorene-based conjugated polymers. Adv Funct Mater 2007;17:71.
[12] Jacob J, Zhang J, Grimsdale AC, Müllen K, Gaal M, List EJW. Poly(tetraarylindenofluorene)s: new stable blue-emitting polymers. Macromolecules 2003;36:8240.
[13] Ouisse T, Stéphan O, Armand M. Degradation kinetics of the spectral emission in polyfluorene light-emitting electro-chemical cells and diodes. Eur Phys J Appl Phys 2003;24:195.
[14] Chen Zhenyu, Ma D. Improved color purity and efficiency in polyfluorene-based light emitting diodes. Mater Sci Eng B 2007;141:71–5.
[15] Mallavia R, Montilla F, Pastor I, Velasquez P, Arredondo B, Alvarez AL, et al. Characterization and side chain manipulation in violet-blue Poly-[(9,9-dialkylfluoren-2,7-diyl)-alt-co-(benzen-1,4-diyl) backbones. Macromolecules 2005;38:3185.
[16] Alvarez AL, Arredondo B, Romero B, Gutiérrez-Llorente A, Quintana X, Mallavia R, et al. Analytical evaluation of the ratio between injection and space-charge limited currents in single carrier organic diodes. IEEE Trans Electron Dev 2008;55(2):674–80.
[17] Gartner F. A comparison of the electrical properties of polymer LEDs based on poly(thiophene)s and PPV-derivatives. PhD thesis, University of Groningen, The Netherlands, 1997.
[18] Khan RUA, Bradley DDC, Webster MA, Auld JL, Walker AB. Degradation in blue-emitting conjugated polymer diodes due to loss of ohmic hole injection. Appl Phys Lett 2004;84:921–3.
[19] Gomes HL, Stallinga P, Cölle M, de Leeuw DM, Biscarini F. Electrical Instabilities in organic semiconductors caused by trapped supercooled water. Appl Phys Lett 2006;88:082101.
[20] Montilla F, Frutos LM, Mateo CR, Mallavia R. Fluorescence emission anisotropy coupled to an electrochemical system: study of exciton dynamics in conjugated polymers. J Phys Chem C 2007;111:18405.
[21] Arkhipov VI, Emelianova EV, Tak YH, Bässler H. Charge injection into light-emitting diodes: theory and experiment. J Appl Phys 1998;84:848.
[22] Yan H, Scott BJ, Huang Q, Marks T. Enhanced polymer light-emitting diode performance using a crosslinked-network electron-blocking interlayer. Adv Mater 2004;16:1948–52.
[23] Bässler H, tak YH, Khramtchenkov DV, Nikitenko VR. Model sof organic light-emitting diodes. Synth Met 1997;91:173–9.
[24] Savvate'ev V, Friedl JH, Zou L, Shinar J, Christensen K, Oldham W, et al. Nanosecond electroluminescence spikes from multilayer blue 4,4′-bis(2,2′-diphenyl vinyl)-1,1′-biphenyl (DPVBi) organic light-emitting devices. Mater Sci Eng 2001;B85:224–7.
[25] Yilmaz Kaptan H. ESR study on the effect of temperature on the diffusion of oxygen into PMMA and PVAc polymers. J Appl Polym Sci 1999;71:1203–7.